Acoustics of the human middle-ear air space

Cara E. Stepp
Picker Engineering Program, Smith College, 51 College Lane, Northampton, Massachusetts 01063 and Speech and Hearing Biosciences and Technology Program, Harvard-M.I.T. Division of Health Sciences and Technology, Cambridge, Massachusetts 02139

Susan E. Voss[a)]
Picker Engineering Program, Smith College, 51 College Lane, Northampton, Massachusetts 01063

(Received 18 January 2005; revised 19 May 2005; accepted 26 May 2005)

The impedance of the middle-ear air space was measured on three human cadaver ears with complete mastoid air-cell systems. Below 500 Hz, the impedance is approximately compliance-like, and at higher frequencies (500–6000 Hz) the impedance magnitude has several (five to nine) extrema. Mechanisms for these extrema are identified and described through circuit models of the middle-ear air space. The measurements demonstrate that the middle-ear air space impedance can affect the middle-ear impedance at the tympanic membrane by as much as 10 dB at frequencies greater than 1000 Hz. Thus, variations in the middle-ear air space impedance that result from variations in anatomy of the middle-ear air space can contribute to inter-ear variations in both impedance measurements and otoacoustic emissions, when measured at the tympanic membrane. © *2005 Acoustical Society of America.* [DOI: 10.1121/1.1974730]

PACS number(s): 43.64.Bt, 43.64.Ha [WPS] Pages: 861–871

I. INTRODUCTION

The human middle-ear air space, schematized in Fig. 1 (left), consists of the tympanic cavity, aditus ad antrum, the antrum of the mastoid, and the mastoid air cells (e.g., Donaldson *et al.*, 1992, p. 151). The tympanic cavity houses the ossicular system and lies between the tympanic membrane and the inner ear. The posterior-superior portion of the tympanic cavity narrows into the passage called the aditus ad antrum which extends to the antrum. Attached to the antrum is a system of mastoid air cells that communicate with one another and vary in size (Donaldson *et al.*, 1992). The total volume of the middle-ear air space is highly variable among normal-hearing ears. The tympanic cavity has a volume ranging from 0.5 to 1 cm^3 (i.e., Gyo *et al.*, 1986; Whittemore *et al.*, 1998); the mastoid air cell system has a much wider volume range, reported[1] by Molvaer *et al.* (1978) to be about 1 to 21 cm^3 and by Koç *et al.* (2003) to be 4 to 14 cm^3.

Even though the large range in middle-ear air space volume is well documented, the acoustical effects of this air space on sound transmission through the human middle ear have not been characterized. Mathematical models of the human middle ear (e.g., Zwislocki, 1962; Kringlebotn, 1988) include the effects of the middle-ear air space (i.e., middle-ear cavity), but because the influence of the air space within these models has a minimal effect on the impedance at the tympanic membrane, the acoustical effects of the middle-ear air space have been largely ignored. For example, as stated by Zwislocki (1962):

> "Since the impedance of the middle-ear cavities is low by comparison to other parts of the middle ear, its effect on the impedance at the eardrum and on the sound transmission to the inner ear is not critical. As a consequence, the analog [model] may be regarded as a sufficient approximation."

The analog circuit model descriptions of the middle-ear cavity of both Zwislocki (1962) and Kringlebotn (1988) are based on measurements of the middle-ear air space impedance that were made on one cadaver ear by Onchi (1961). The only subsequent measurements of middle-ear air space impedance were made on cadaver ears that lacked a portion of their mastoid air-cell networks (Voss *et al.*, 2000b). The goal of this work is to describe the acoustics of the normal (unaltered) middle-ear air space.

Although the role of the human middle-ear air space has been largely ignored in normal ears, its acoustical effects are known to be important in determining middle-ear sound transmission in several pathological middle-ear conditions. For example, Merchant and colleagues have demonstrated that in type IV and type V tympanoplasties, the air space between the graft shield and the round window (termed the cavum minor) should be maximized in order to maximize hearing (Rosowski and Merchant, 1995; Rosowski *et al.*, 1995; Merchant *et al.*, 1995, 1997, 1998). Voss and colleagues have shown that (1) the volume of the middle-ear air space plays a major role in middle-ear function in ears with tympanic membrane perforations (or tubes) at frequencies below about 1000 Hz (Voss, 1998; Voss *et al.*, 2001a, b, c) and (2) in some pathological ears, the air volume and anatomy of the middle-ear air space can influence the sound produced by audiological earphones (Voss *et al.*, 2000a, c).

The work reported here is a step toward a description of the acoustics of the human middle-ear air space. Specifically, we report measurements, made on human cadaver ears, of the impedance of the human middle-ear air space, and we use these measurements in combination with previous measurements and models to predict how the middle-ear air

[a)]Electronic mail: svoss@email.smith.edu

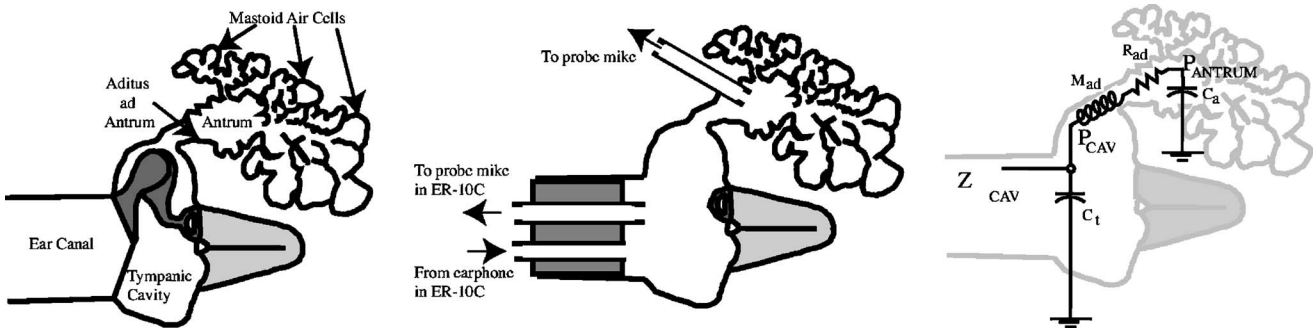

FIG. 1. **Left Panel:** Schematic of the air spaces of the human middle-ear. The tympanic cavity houses the ossicles and is connected to the mastoid air cells and antrum by the tube-like aditus ad antrum. Adapted from Onchi (1961). **Middle Panel:** Schematic of the measurement setup. The tympanic membrane, malleus, and incus are removed. The sound source and microphone assembly sit in the ear canal with the probe tube of the microphone flush with the entrance to the tympanic cavity and extended about 3 mm from the sound tube. To measure the antrum pressure, a probe tube connected to a microphone sits in the antrum. **Right Panel:** An analog circuit model schematic of the middle-ear air space (e.g., Zwislocki, 1962; Kringlebotn, 1988; Voss *et al.*, 2000b). The circuit model relates to the ear structure through the location of circuit elements on the structural outline. The voltages are analogous to sound pressures and currents are analogous to volume velocities. The capacitor in the tympanic cavity represents the volume of air in the tympanic cavity, the resistor and inductor within the additus ad antrum represent the tube-like passage, and the capacitor in the antrum represents the volume of air in the antrum and mastoid air cells.

space does affect the impedance at the tympanic membrane. Our results suggest that the middle-ear air space in normal ears may play a role in some of the variability observed in ear-canal based acoustical measurements on normal populations; such variations among normal ears are essential to understand as otoacoustic emissions and middle-ear power flow measurements are developed as clinical tools (e.g., Stinson, 1990; Keefe *et al.*, 1993; Voss and Allen, 1994; Keefe and Levi, 1996; Hunter and Margolis, 1997; Margolis *et al.*, 1999; Piskorski *et al.*, 1999; Feeney and Keefe, 1999, 2001; Farmer-Fedor and Rabbitt, 2002; Feeney *et al.*, 2003; Magliulo *et al.*, 2004). A preliminary account of this work has been presented elsewhere (Stepp and Voss, 2004).

II. METHODS

A. Cadaver-ear preparation

Comparisons of measurements of acoustic impedance (Rosowski *et al.*, 1990) and of umbo velocity (Goode *et al.*, 1993) between populations of cadaver ears and living ears show no significant differences between the two populations. This apparent normality of acousto-mechanical properties for cadaver ears supports our assumption that the middle-ear air space impedance in the cadaver preparation is equivalent to that in live human ears.

Four adult human hemi-heads that included the entire temporal bone, mastoid air space, and external ear were obtained through the nonprofit organization Life Legacy. Specimens were frozen after removal from their donor, shipped on dry ice, and put in the freezer upon arrival. The first ear was used to develop the methods, and measurements are reported on the final three ears, labeled ears 1, 2, and 3 here. We note that ears 2 and 3 are the right and left ears, respectively, from the same subject. To prepare the ears for measurement, each specimen was thawed and reduced to a manageable size by sawing away bony areas not relevant for the measurements. The entire mastoid space, including all mastoid air cells, was left intact. Next, the bony ear canal was drilled away so that the tympanic ring was fully exposed. Using an otologic-operating microscope, the tympanic membrane, malleus, and incus were removed with forceps, and the stapes was left in the oval window of the cochlea to prevent leakage of cochlear fluid (Fig. 1 middle). In all cases, the ears appeared normal. At this point in the preparation, the ears were refrozen. Several weeks later they were thawed by placing them in a saline-filled container for several hours and measurements were made after they thawed and the saline was suctioned away.

A cylindrical coupling ring designed to couple the sound source to the tympanic ring was attached to the tympanic ring with carboxylate dental cement (ESPE, Durelon, Norristown, PA). This coupling ring had an inner diameter of 11 mm, which approximated the size of the tympanic rings in our specimens. Any irregular spaces between the ring and the bone were filled with dental cement. When the sound source was coupled to the tympanic ring via the coupling ring, the tip of the probe-tube microphone extension (Sec. II C) was approximately at the same depth as the tympanic ring (Fig. 1 middle). To ensure that the middle-ear was sealed acoustically, much of the specimen was coated with additional dental cement, and the specimen was also placed in the finger of a latex glove that provided a tight fit around it. Prior to making acoustic measurements, suction was applied to both the tympanic cavity and the antrum (via the aditus ad antrum) to remove any fluid (i.e., saline) that had collected in the middle-ear air space.

In one ear (ear 3), a probe-tube for a microphone (Etymōtic Research ER-7C) was secured in the antrum in order to measure the sound pressure at this location. In this case, a narrow (less than 1 mm in diameter) tube-like hole was drilled in the roof of the antrum. A flexible probe tube (Etymōtic Research) was secured with dental cement through this hole in the antrum. The location was confirmed visually by looking through the tympanic ring and aditus ad antrum and observing that the tip of the probe-tube sat within the antrum.

B. Stimulus generation and response

The software package SYSid was used to obtain complex frequency response measurements. The stimulus was a broad-band chirp (25 Hz to 25 kHz), and the response mag-

nitudes and angles were calculated as the 2048-point FFT of the time-domain average of N responses. Measurements were sampled at 50 kHz, with $N=1000$ and an input voltage of 0.4 V, which was found to be within the linear operation range for all measurements made.

The acoustic assembly coupled to the tympanic ring was an ER-10C (Etymōtic Research), which contains both a sound source to transduce the computer-generated voltage signal to an acoustic signal and a microphone to transduce the sensed sound to a voltage. The ER-10C was driven by SYSid, and the microphone's response was recorded via this same system. The ER-10C was coupled to either the ear or the calibration cavities (Sec. II C).

C. Impedance measurements

The acoustic assembly was characterized by its Thévenin equivalents, P_{TH} and Z_{TH}, using a method similar to that of Allen (1986), Voss and Allen (1994), and Neely and Gorga (1998). The acoustic assembly was coupled to loads with known acoustic impedance, and microphone responses to the chirp stimulus were measured for each load. The loads were cylindrical closed-ended tubes of different lengths, each with a known theoretical impedance determined by the equations developed by Keefe (1984). The loads all had an inner diameter of 11 mm and lengths ranged from 1.14 to 4.41 cm. The acoustic assembly was coupled to the loads via a cylindrical plastic adapter that housed both the sound-delivery tube and the microphone probe tube of the ER-10C and was machined to fit snugly into each load while maintaining a constant inner diameter of 11 mm. The same plastic adapter fit snugly to the acoustic coupler that was cemented to the tympanic ring. This coupling arrangement allowed for measurements on ears and cylindrical loads without changing the relative position of the microphone with respect to the sound-delivery tube. To minimize the contribution of nonuniform waves generated at the earphone tube tip (e.g., Huang *et al.*, 2000), a small piece of tygon tubing was used to extend the microphone probe tube beyond the sound-delivery tube by 3 mm for all measurements (in loads and in ears).

Measurements were made in nine loads (cylindrical tubes). Four of these responses were used to determine the Thévenin equivalents, P_{TH} and Z_{TH}. These four responses, in combination with the theoretical load impedances, provided an over-specified set of four equations that were solved in MATLAB by optimizing the lengths of the cavities in order to minimize the least-squares error between the four equations and to solve for P_{TH} and Z_{TH} (e.g., Allen, 1986; Voss and Allen, 1994; Neely and Gorga, 1998). Measurements made on the additional five loads were used as controls; measurements in these five loads were used in combination with the determined P_{TH} and Z_{TH} to calculate a measured impedance for each load, which was compared with the theoretical impedance. The ratio between the measurements and the theory generally had a magnitude of less than 1 dB and an angle difference of less than 0.025 cycles; larger differences occurred only at the frequencies where the impedance magnitude was a maximum or minimum. These comparisons suggest that the impedance measurements are generally accurate to within about 10% in magnitude (about 1 dB) and 10° in angle (0.025 cycles).

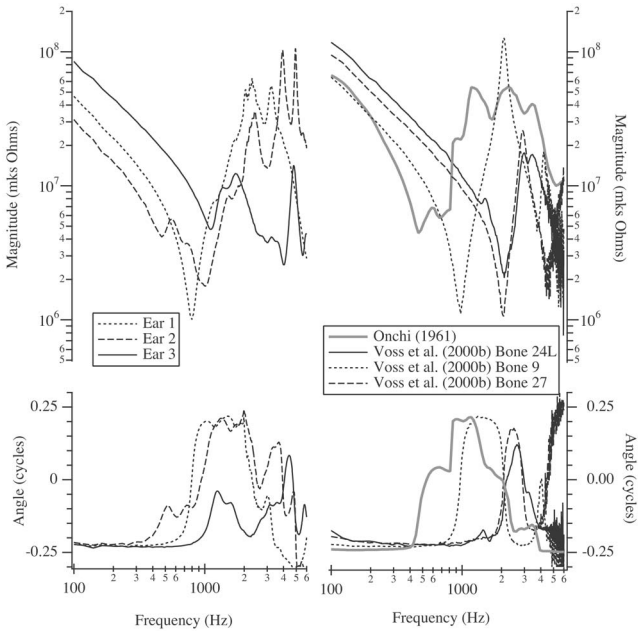

FIG. 2. Acoustic impedances of the middle-ear air space Z_{CAV}. **Upper Panel:** Impedance magnitudes. **Lower Panel:** Impedance angles. **Left Panel:** Impedances measured on the three ears reported here. **Right Panel:** Measurements of middle-ear air space impedance from Onchi (1961) (N =1) and Voss *et al.* (2000b). Three representative measurements of 11 total measurements from Voss *et al.* (2000b) are shown; all other measurements exhibit similar features to these three.

D. Measurement of antrum pressure

Responses to a chirp stimulus delivered to ear 3 were recorded simultaneously from a probe-tube microphone (ER-7C) inserted into the antrum and the ER-10C microphone at the tympanic ring. The antrum microphone (ER-7C) was calibrated with respect to the ER-10C microphone (microphone at the tympanic ring) via a measurement made with the two microphones adjacent to each other in a single airtight cavity. The voltages from both microphones were measured simultaneously in response to a chirp stimulus, and the ratio between the two microphone responses was used to calibrate the antrum microphone (ER-7C) relative to the tympanic-ring microphone (ER-10C).

III. RESULTS

A. Impedance of the middle-ear air space: Z_{CAV}

The acoustic impedances (Z_{CAV}) of the middle-ear air spaces have similar features for all three ears (Fig. 2 left). Below 500 Hz, all ears are compliance dominated with a decrease in impedance magnitude of 20 dB per decade and a near constant angle of about −0.25 cycles. At frequencies between 500 and 6000 Hz, the magnitudes have five to nine local extrema associated with steep changes in phase angle. Two of the three impedances have a mass-dominated region centered at about 1000 Hz, with a magnitude that increases at 20 dB per decade and an angle that approaches 0.25 cycles.

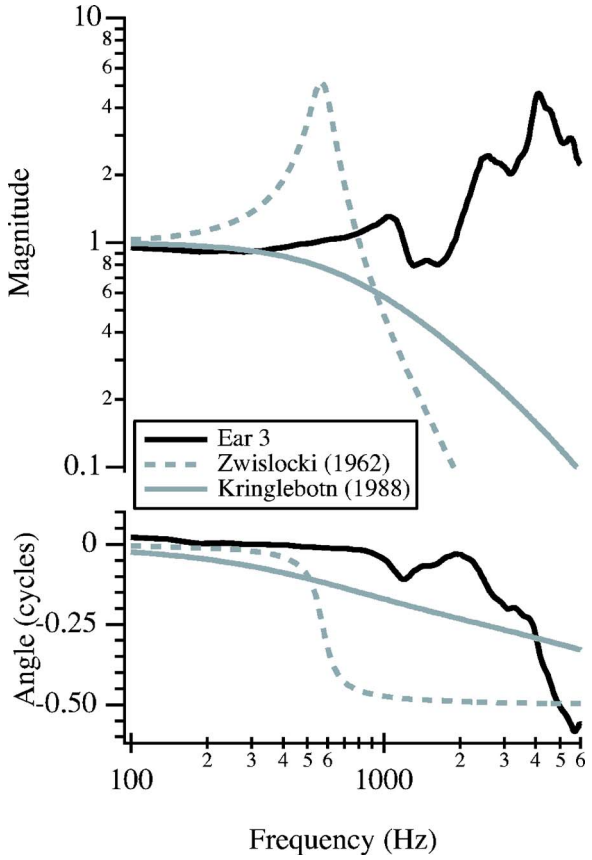

FIG. 3. A measurement of H_P, the ratio between the pressure in the antrum, P_{ANTRUM}, and the pressure at the tympanic ring, P_{CAV}, where $H_P = P_{\mathrm{ANTRUM}}/P_{\mathrm{CAV}}$, for ear 3. Also plotted are the model results of H_P from both Zwislocki (1962) and Kringlebotn (1988).

As frequency increases above 1000 Hz, none of the impedances can be described in terms of simple behavior (i.e., compliance, resistance, or mass dominated).

B. The antrum transfer function

In one ear (ear 3), the pressure in the antrum of the mastoid, P_{ANTRUM}, and the pressure at the tympanic ring, P_{CAV}, were measured simultaneously. The ratio between these pressures,

$$H_P = \frac{P_{\mathrm{ANTRUM}}}{P_{\mathrm{CAV}}}, \tag{1}$$

is plotted in Fig. 3. At low frequencies, the magnitude of H_P is nearly one and the angle is nearly zero. Thus, for these low frequencies, $P_{\mathrm{ANTRUM}} \approx P_{\mathrm{CAV}}$. As frequency increases, P_{ANTRUM} and P_{CAV} differ, and $|H_P|$ exhibits several local extrema.

IV. DISCUSSION

A. Measurements of Z_{CAV}

Previously published measurements of the middle-ear air space impedance (Z_{CAV}) include one measurement from Onchi (1961) and eleven measurements from Voss *et al.* (2000b). The measurement from Onchi (1961) appears to have included the entire mastoid space.[2] The eleven ears used by Voss *et al.* (2000b) were removed with a circular saw (Schuknecht, 1968) such that much of the mastoid air-cell network was left with the cadaver and was not part of the ear specimen used for measurement; thus, these eleven ears had smaller-than-normal mastoid volumes and air-cell networks—we will refer to this condition as "altered mastoid."

The middle-ear air space impedances measured here (Fig. 2 left) show both similarities and differences to the other measurements (Fig. 2 right). Many features are consistent among all measurements: (1) low-frequency behavior is compliance dominated; (2) low-frequency magnitudes are similar; and (3) above 500 Hz there are extrema in magnitude that are associated with steep changes in phase angle. There are also some differences between the measurements made with the unaltered mastoid system [i.e., measurements made here and by Onchi (1961)] as compared to the measurements from Voss *et al.* (2000b) with altered mastoids. Above 500 Hz, the measurements with unaltered mastoids have a mixed impedance, characterized by several (i.e., five to nine) extrema in magnitude with associated steep changes in phase angle. In contrast, the measurements with the altered mastoids (Voss *et al.*, 2000b) show fewer extrema in magnitude; specifically, there are two extrema between 100 and 4000 Hz—one sharp magnitude minimum and one sharp magnitude maximum, both with associated steep changes in phase angle.[3] Thus, the unaltered and altered mastoid cavity configurations are not equivalent to one another; in the following, we explore how their differences affect both middle-ear models and measurements of impedance.

B. Modeling Z_{CAV}

Analog circuit models of the middle-ear air space were reviewed by Voss *et al.* (2000b) and are briefly summarized here. The models of Zwislocki (1962), Kringlebotn (1988), and Voss *et al.* (2000b) are designed to represent the structure/function relationship of the middle-ear air space, and a summary of these models is shown in the right panel of Fig. 1.[4] The models employ a capacitor to represent the compliance of air in the tympanic cavity. This capacitor is in parallel with a series resistor-inductor-capacitor connection. The resistor-inductor path represents volume velocity flow through the tube-like additus ad antrum and the capacitor represents the compliance of the air in the antrum and mastoid air cavities. The models do not include components to represent the acoustics of the air-cell tracts throughout the mastoid. With three energy storage elements, this four-element topology includes two distinct resonances in the impedance of the middle-ear air space: (1) a minimum in impedance magnitude is determined by a series resonance between the inductor and the capacitor that represents the antrum air volume, and (2) a maximum in magnitude impedance is determined by a parallel resonance between the inductor and the combination of the two capacitors.[5] This general four-element model topology has been successfully applied to represent impedance measurements on both human cadaver ears with the mastoid air-cell tract mostly re-

TABLE I. Middle-ear cavity model parameters. Volumes are estimated from the model-compliance values using the relationship $V=\rho c^2 C$ where C is the compliance of air within the volume V, ρ is the density of air, c is the speed of sound in air, and f is frequency in Hz. Bone 24L is used as a representative bone (of 11 total) because it was the one analyzed in detail in Voss *et al.* (2000b).

Ear(mks units)	R_{ad}	M_{ad}	C_a	C_t
Ear 1 Stepp and Voss	$0.03\times10^6\sqrt{f}$	1276	2.9×10^{-11} $V=4.0$ cm^3	5.2×10^{-12} $V=0.73$ cm^3
Ear 2 Stepp and Voss	$0.06\times10^6\sqrt{f}$	550	4.2×10^{-11} $V=5.9$ cm^3	8.8×10^{-12} $V=1.24$ cm^3
Ear 3 Stepp and Voss	$0.15\times10^6\sqrt{f}$	1857	1.0×10^{-11} $V=1.5$ cm^3	6.7×10^{-12} $V=0.94$ cm^3
Bone 24L Voss *et al.* (2000b)	$0.05\times10^6\sqrt{f}$	890	6.3×10^{-12} $V=0.9$ cm^3	6.3×10^{-12} $V=0.9$ cm^3
Range ($N=11$) Voss *et al.* (2000b)	$0.02\times10^6\sqrt{f}-0.08\times10^6\sqrt{f}$	520–1420	$4.2\times10^{-12}-18.8\times10^{-12}$ $V=0.6$ to 2.6 cm^3	$2.5\times10^{-12}-8.0\times10^{-12}$ $V=0.4$ to 1.1 cm^3

moved (Voss *et al.*, 2000b) and on cat ears (Huang *et al.*, 1997), in which two cavities are connected by an additus-like tube and no mastoid air cells are present.

We fit the four-element model (Fig. 1 right) to the measurements made here using the same procedure outlined by Voss *et al.* (2000b), which is summarized in the Appendix. Voss *et al.* (2000b) applied this procedure to each of the 11 bones for which Z_{CAV} with an altered mastoid space was measured. Here, we apply the same procedure to the 3 ears for which Z_{CAV} was measured with an unaltered mastoid space; the specific model elements are listed in Table I along with the predicted volumes for the tympanic and mastoid air spaces.[6] Figure 4 shows comparisons between the four-element model and the measured Z_{CAV} from the three ears here with unaltered mastoids and two ears (B24L and B13) with altered mastoids from Voss *et al.* (2000b). Voss *et al.* (2000b) describe the model fit to the data for ears with altered mastoids:

> In general, below 3000 Hz, the model captures most salient features of the data. At the lowest frequencies, the model angle is nearly −0.25 while the data angle is about −0.20 cycles. Across our population of 11 ears, some of the low-frequency Z_{CAV} angles are at −0.25 cycles while others approach −0.20 cycles; reasons for the difference are not clear. Above 3000 Hz, our model and the data diverge. The local maximum in the data, near 3000 Hz, is overestimated by the model. Thus, up to 3000 Hz, the model is a reasonable description of the measured Z_{CAV}.

In contrast to the measurements with the altered mastoid, the four-element model is unable to fit the Z_{CAV} measured on ears with unaltered mastoids as well as it fits ears with altered mastoids. The three measurements with Z_{CAV} from the unaltered mastoid state (Fig. 4, ears 1, 2, and 3) show that the four-element model is able to represent the Z_{CAV} behavior at the lower frequencies (e.g., less than 500 Hz) and is able to capture the general behavior of the first minimum in magnitude. However, at frequencies near and above the first minimum in magnitude, the four-element model is unable to capture any of the fine structure of the multiple extrema in the measured Z_{CAV}.

In summary, the model topology of Fig. 1 (right) describes the general features of Z_{CAV} for ears with both intact and altered mastoid cavities, but it does not describe all features of the measurements with unaltered mastoids [made both here and by Onchi (1961)[7]], with the mastoid air-cell tract intact. The three energy-storage elements in the model limit the model to two distinct resonances. However, all measurements made with an intact mastoid air-cell system suggest multiple resonances above about 1000 Hz. It appears

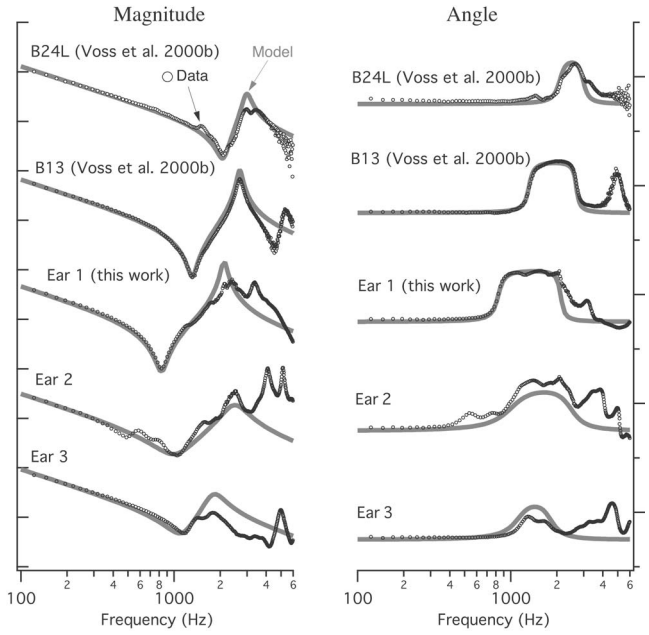

FIG. 4. Comparisons of measurements of Z_{CAV} to the four-element model (Fig. 1 right). Model element values were calculated for each ear via the process outlined in the Appendix. The measured Z_{CAV} (data) are plotted with open black circles and the corresponding model fits are plotted with a gray solid line. The upper two examples are from ears with altered mastoid cavities (Voss *et al.*, 2000b), and the lower three examples are from the ears presented here with normal mastoid cavities. To improve visibility, the plots were shifted on the same graphs and thus the exact values are not labeled. **Left Panel:** Magnitudes. **Right Panel:** Angles.

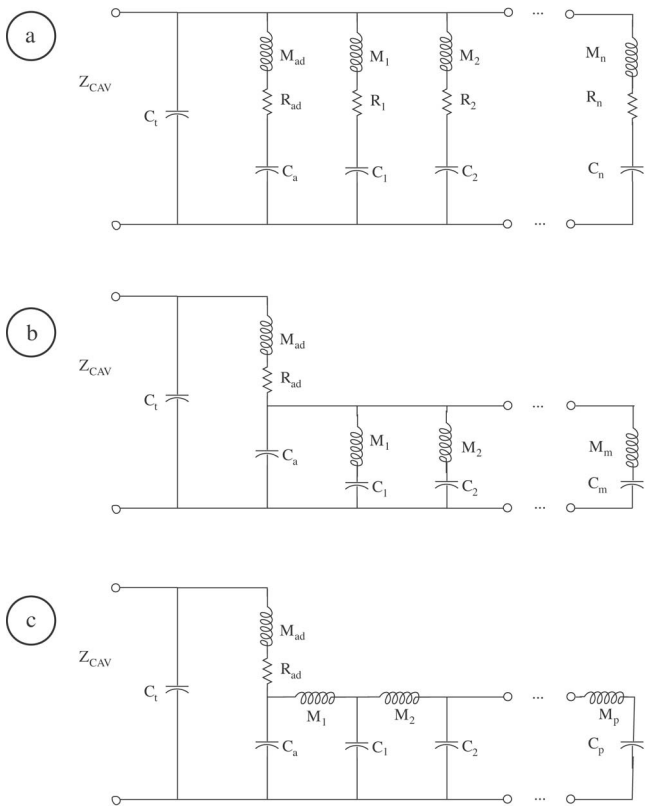

FIG. 5. Analog circuit models that represent features of the middle-ear air space. All three models (a, b, and c) include the four elements (C_t, M_{ad}, R_{ad}, and C_a) of the model described in Fig. 1 (right). A model for the middle-ear air space might include all three mechanisms represented here through three individual topologies. **(a)** Connections between the tympanic cavity and the mastoid air-cell system in addition to the aditus ad antrum are represented by series connections between a mass, a resistor, and a compliance. The model represents a total of n such connections. **(b)** The model represents m tracts within the mastoid air-cell system that originate at the antrum and terminate with a volume of air. **(c)** The model represents a single air-cell tract that originates at the antrum and progressively narrows. This model represents the narrowing of a single air-cell tract through connections of p masses and compliances.

that a more complicated model—possibly such as the "transmission line model" suggested by Onchi (1961)—is needed if the goal is to represent all extrema in the impedance magnitude of the intact middle-ear air space of the human ear.

A model of the middle-ear air space that accounts for more features than the simple four-element model accounts for would be highly individual, as the structure of each individual's mastoid air-cell system is unique (Molvaer *et al.*, 1978). The measurements here show that such a model would have several extrema in the impedance magnitude, and the specific number would depend on the individual ear (e.g., Fig. 2). Figure 5 schematizes three possible model topologies that relate structure to function of the middle-ear air space; these models are described to represent possible structure/function relationships within the middle-ear air space, but they are not detailed precise models of any particular middle-ear air space. In fact, a model of a specific middle-ear air space would most likely be a combination of all three of these model topologies. All three models of Fig. 5 include the four elements (C_t, M_{ad}, R_{ad}, and C_a) of the model described in Fig. 1 (right), which has been successfully used to represent the impedance of ears with altered mastoids. Figure 5(a) represents connections between the tympanic cavity and the mastoid air-cell system that are in addition to the aditus ad antrum. Specifically, each series connection between a mass, resistor, and compliance represents a "tube-like" connection from the tympanic cavity to a volume of air within the mastoid air-cell system. The model represents a total of n such connections.[8] Figure 5(b) is the "transmission line model" suggested by Onchi (1961). The model represents m tracts within the mastoid air-cell system that originate at the antrum and terminate with a volume of air; the model does not represent that each air-cell tract generally gets smaller as it moves away from the antrum. Figure 5(c) represents a single air-cell tract that originates at the antrum; each mass attached to a compliance represents a short tube-like structure that terminates with a volume in which air can compress and expand. Attached to that volume is an additional short tube-like structure that in turn is terminated with a volume. This model can represent the narrowing of a single air-cell tract through connections of p masses and compliances, and the specific values for the masses and compliances depend upon the dimensions of the air-cell tract being modeled. In summary, a model of the mastoid air-cell system that represents all extrema in the measured impedance would most likely include a combination of the mechanisms represented by the three models of Fig. 5. We do not propose that such a model is particularly useful, as we expect the model would be substantially different for each individual ear. However, the topologies in Fig. 5 provide an outline for how one might think about the acoustics of the middle-ear air space and the multiple and variable number of extrema in the measured impedances.

C. Effect of the middle-ear air space on the impedance at the tympanic membrane

To date, our knowledge of how the middle-ear air space impedance affects the impedance of the middle ear at the tympanic membrane has been based on middle-ear models. As discussed earlier (Sec. IV B), these models do not represent all features of the impedance of the middle-ear air space. Here, we use the measurements of the middle-ear air space impedance Z_{CAV} to estimate how variations in middle-ear air space impedance affect the impedance of the ear at the tympanic membrane. We assume that

$$Z_{TM} = Z_{TOC} + Z_{CAV}, \tag{2}$$

where Z_{TM} is the impedance at the tympanic membrane, Z_{TOC} is the impedance of the tympanic membrane, ossicles, and cochlea, and Z_{CAV} is the impedance of the middle-ear air space. Equation (2) is equivalent to middle-ear models in which the middle-ear air space (e.g., cavity) is represented by Z_{CAV} and is in series with the rest of the ear, represented as Z_{TOC} (e.g., Zwislocki, 1962; Kringlebotn, 1988; Voss *et al.*, 2001c). The use of Eq. (2) allows us to determine how Z_{TM} is affected by Z_{CAV}; in particular, estimates of Z_{TM} from the same ear or model can be made using a measured or modeled Z_{TOC} with a variety of representations of Z_{CAV} so that the effect of Z_{CAV} can be understood.

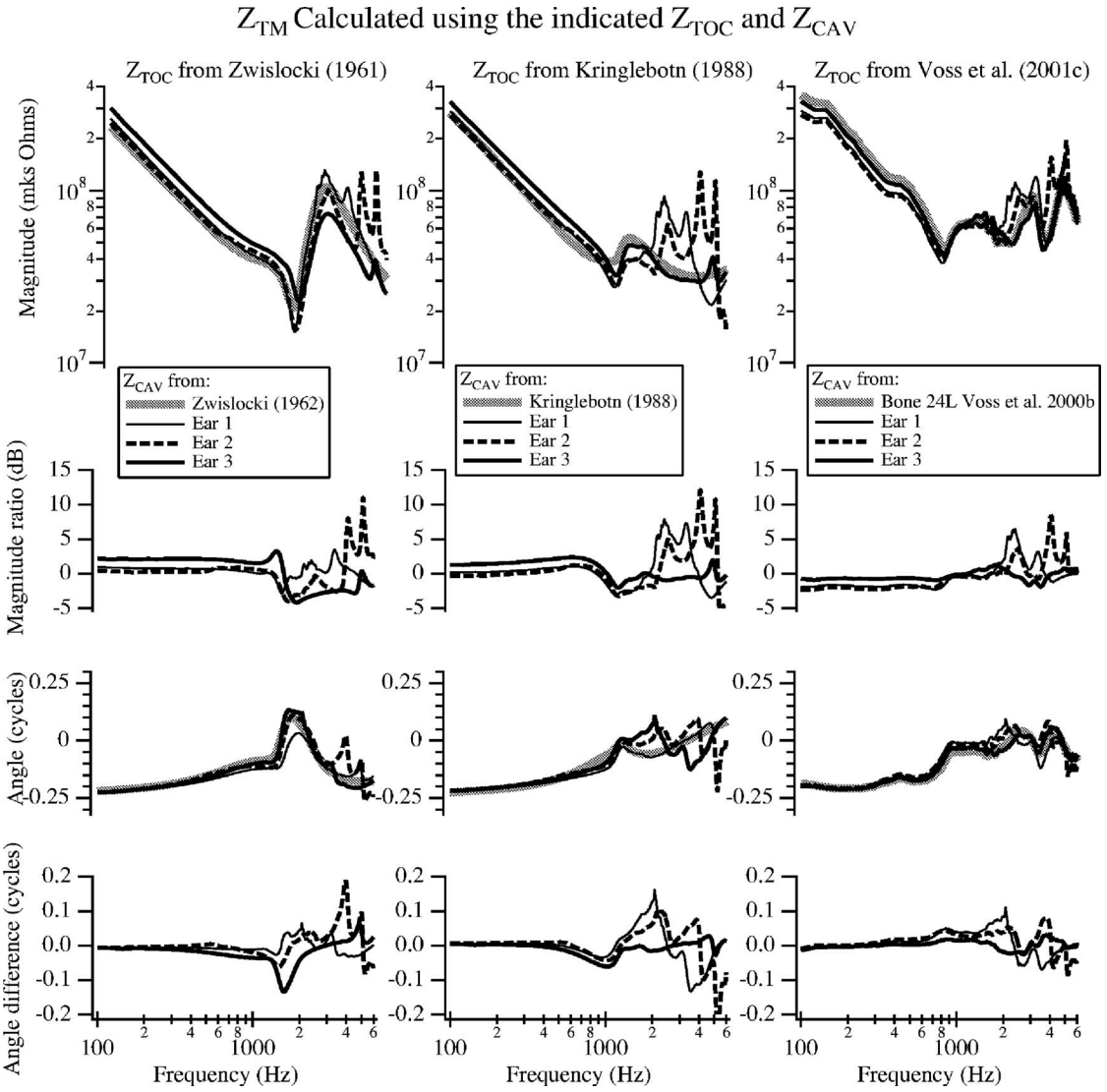

FIG. 6. Model results of the impedance at the tympanic membrane, Z_{TM}, calculated from Eq. (2), using different values for the impedance of the tympanic membrane, ossicles, and cochlea, Z_{TOC}, and the impedance of the middle-ear air space, Z_{CAV}. The values of Z_{TOC} were calculated from: **Left Panel:** the model of Zwislocki (1962); **Middle Panel:** the model of Kringlebotn (1988); and **Right Panel:** the measurements of Voss *et al.* (2001c). The values of Z_{CAV} used for each Z_{TM} calculation are indicated in the legends and were either calculated using the relevant model formulation or are measurements from this work (ears 1, 2, and 3) or from Bone 24L of Voss *et al.* (2001b). **Upper:** Magnitude of the impedance at the tympanic membrane with the indicated Z_{TOC} and Z_{CAV}. **Middle-upper:** Magnitude ratio between the calculation with the Z_{CAV} from the ears with unaltered mastoids (ears 1, 2, and 3) and the baseline load (Zwislocki model, Kringlebotn model, and Bone 24L), where the ratio is plotted in dB where the ratio is computed as 20 $\log_{10}(Z_{CAV}/Z_{CAV}^{baseline})$. **Middle-lower:** Angle of the impedance at the tympanic membrane with the indicated Z_{TOC} and Z_{CAV}. **Lower:** Difference in angle between the calculation with the Z_{CAV} from the ears with unaltered mastoids (ears 1, 2, and 3) and the baseline load (Zwislocki model, Kringlebotn model, and Bone 24L).

We calculate the impedance at the tympanic membrane (Z_{TM}) from Eq. (2) using a combination of models and measurements of Z_{TOC} and Z_{CAV}. Specifically, we use three different estimates of Z_{TOC}: (1) Z_{TOC} from the Zwislocki (1962) model, (2) Z_{TOC} from the Kringlebotn (1988) model, and (3) the measurements of Z_{TOC} from Voss *et al.* (2001c). In combination with these estimates of Z_{TOC}, we use the middle-ear air space impedance Z_{CAV} as determined from the Zwislocki (1962) model, the Kringlebotn (1988) model, the measurements of Voss *et al.* (2000b), and the measurements of Z_{CAV} presented here. Figure 6 plots the impedance at the tympanic membrane, Z_{TM}, using these combinations of Z_{TOC} and Z_{CAV}. The middle-ear air space does affect the impedance at the tympanic membrane. Low-frequency differences between the results with the model air-space impedance and the measured air-space impedance occur because the total volume of the air space differs between the three measurements and the target volume of each model. Above 1000 Hz the major results include: (1) the introduction of multiple maxima and minima in the impedance at the tympanic membrane when Z_{CAV} comes from the impedance measured on ears with unaltered mastoid cavities (i.e., ears 1, 2, 3 versus the models or the altered mastoid cavity of bone 24L), and (2) variations of more than 10 dB in magnitude and 0.1 cycles in angle from the impedances predicted by either model. The introduction of multiple maxima and minima is consistent with many of the impedance measurements of Voss and Allen (1994, Figs. 6 to 10) in which the advanced impedance (estimate of the impedance at the tympanic membrane) demonstrates multiple local maxima and minima, similar to those seen here in

the model results of Fig. 6. Thus, it appears that variations in human middle-ear air spaces might influence the impedance at the tympanic membrane: (1) below 1000 Hz the effect depends on the total volume of the middle-ear air space and systematically increases or decreases the total magnitude by a few dB at all low frequencies, and (2) above 1000 Hz, the effect is complicated, depends on the specific anatomy of a particular ear, and can introduce multiple maxima and minima as a fine structure in the impedance.

D. What does the antrum transfer function H_P tell us?

1. H_P: Models and measurements

Figure 3 compares our measurement of H_P [Eq.(1)] to the middle-ear circuit models of both Zwislocki (1962) and Kringlebotn (1988). Both models predict one maximum in the magnitude of $|H_P|$ with a decrease in magnitude of 40 dB per decade at frequencies above the maximum. The measurement, on the other hand, has multiple extrema that are not represented by these models. The measurement is consistent with the model topologies of Fig. 5, where multiple extrema result from additional energy-storage elements in the model. We are not aware of any other measurements that compare antrum pressure to other pressures within the middle-ear air space; thus, our single measurement of H_P provides a test of the structure-based middle-ear cavity model that suggests that that mastoid air-cell network is important. This measurement-based result is new and invites more work.

2. Impedance of the antrum and mastoid air-cell system

We use our measurement of H_P, the transfer function between the pressures P_{ANTRUM} and P_{CAV}, to characterize the impedance of the antrum and mastoid air-cell system. Specifically, we propose the model topology of Fig. 7 (upper), which differs from the previous models (i.e., Fig. 1 right) in that the antrum and mastoid air-cell system are not represented by a single capacitor but instead by the impedance Z_{MASTOID}. Using the model topology of Fig. 7 (upper), a measurement-based estimate for Z_{MASTOID} can be calculated as

$$Z_{\mathrm{MASTOID}} = \frac{H_P}{\frac{1}{Z_{\mathrm{CAV}}} - \frac{1}{Z_T}}, \tag{3}$$

where H_P is the measured transfer function between the pressures P_{ANTRUM} and P_{CAV}, Z_{CAV} is the measured impedance of the middle-ear air space impedance, and $Z_T = 1/j\omega C_t$ is the impedance of the tympanic cavity with the compliance of the tympanic cavity C_t determined from the volume of the tympanic cavity[9] and calculated for volumes of 0.5, 1.0, and 1.5 cm^3, which spans the range of tympanic-cavity volumes reported in the literature (Gyo *et al.*, 1986; Whittemore *et al.*, 1998) and estimated from model fits (Table I).

The measurement-based estimate of Z_{MASTOID} (Fig. 7 lower) is not consistent with the previous modeling approach of representing the antrum and mastoid air-cell system by a single compliance (Fig. 1 right). At low frequencies Z_{MASTOID} is compliance dominated, but above about 800 Hz

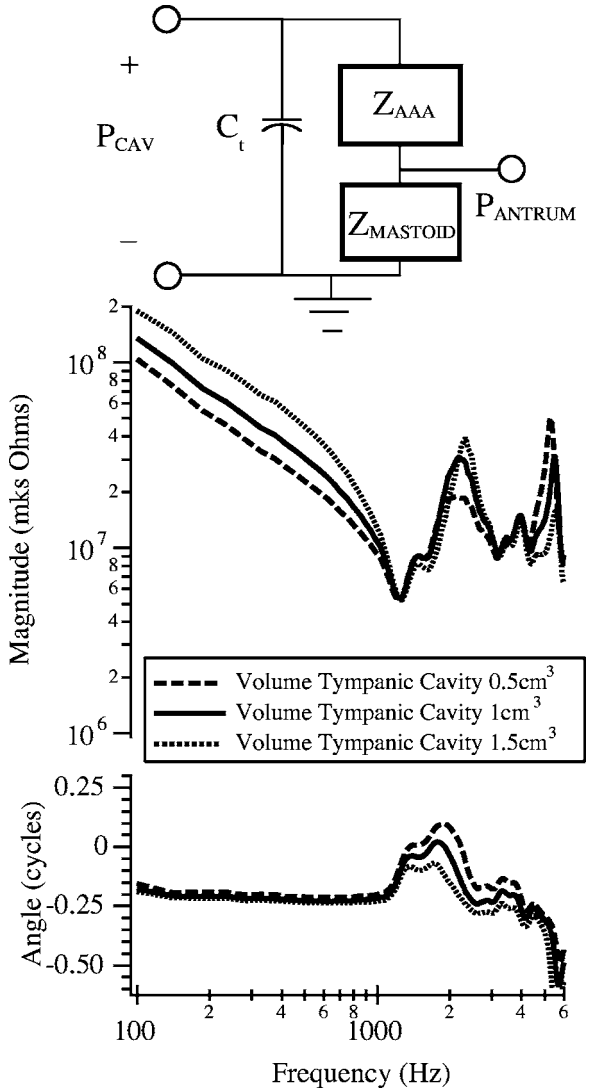

FIG. 7. Estimates of the impedance of the antrum and mastoid air-cell system, Z_{MASTOID}. Z_{MASTOID} is calculated using the model topology shown in the upper panel combined with measurements from ear 3 of the pressure at the tympanic ring, P_{CAV}, and within the antrum, P_{ANTRUM}, and the representation of the tympanic cavity by a compliance C_t. The magnitude (middle panel) and angle (lower panel) of Z_{MASTOID} is plotted for tympanic cavity volumes of 0.5, 1.0, and 1.5 cm^3.

Z_{MASTOID} would be better represented by a model with multiple resonances, such as a combination of the possibilities proposed here in Fig. 5. Above 4000 Hz, our measurement-based estimate of Z_{MASTOID} clearly includes errors, as the angle is less than −0.25 cycles. This error could be due in part to the fact that as frequency increases, the tympanic cavity cannot be represented as a pure compliance. In other words, as the wavelength of sound approaches 10%–20% of the dimensions of the tympanic cavity, it is inappropriate to represent the components as lumped-circuit elements.

E. Clinical implications of results

Many researchers are working to develop noninvasive ear-canal based acoustical measurements as diagnostic tools for middle- and inner-ear dysfunction (e.g., impedance and reflectance measurements, ossicular motion measurements, otoacoustic emissions). It has been noted that substantial

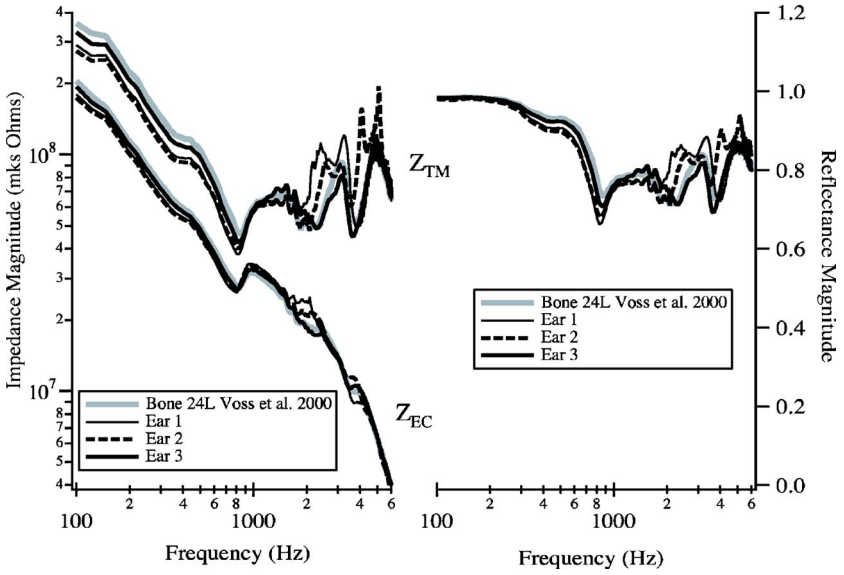

FIG. 8. **Left Panel:** Impedance magnitudes at the tympanic membrane ($|Z_{TM}|$) and 10 mm from the tympanic membrane in the ear canal ($|Z_{EC}|$). The $|Z_{TM}|$ are reproduced from the right column of Fig. 6 and were calculated from Eq. (2) from the Z_{TOC} of bone 24L of Voss *et al.* (2001c) and the Z_{CAV} from the same bone, and ears 1, 2, and 3 here. The $|Z_{EC}|$ was calculated for each $|Z_{TM}|$ by modeling the ear canal as a 10-mm-long air-filled cylindrical tube with a diameter of 8 mm [e.g., Voss and Shera, 2004, Eq. (3)]. **Right Panel:** Reflectance magnitudes calculated from the Z_{EC} at the left, using Eq. (2) of Voss and Allen (1994) (i.e., $R=(Z_{EC}^n-1)/(Z_{EC}^n+1)$, where Z_{EC}^n is the ear-canal impedance normalized by the characteristic impedance of the ear canal).

variability occurs in these measurements in normal-hearing ears (e.g., Zwislocki and Feldman, 1970; Voss and Allen, 1994; Møller, 2000). The work presented here demonstrates that variations in middle-ear air space anatomy contribute to some of the observed intersubject variability in ear-canal based acoustic measurements. Figure 6 demonstrates the effects of variations in middle-ear air space on the impedance at the tympanic membrane: Above 1000 Hz, there are variations of up to 10 dB in magnitude and 0.1 cycles in angle.

Ear-canal based impedance measurements are typically made within the ear canal several millimeters away from the tympanic membrane and not at the tympanic membrane; in this case, the air space between the measurement location and the tympanic membrane contributes substantially to the impedance measurement. Figure 8 (left) compares the impedance magnitude at the tympanic membrane Z_{TM} to the impedance magnitude within the ear canal 10 mm from the tympanic membrane Z_{EC}; variations in middle-ear air space impedance have nearly indistinguishable effects on the impedance at the location 10 mm from the tympanic membrane. Indeed, impedance measured within the ear canal is heavily influenced by the impedance location measurement, and as such, ear-canal impedances are limited in the information they provide. As detailed by others, including Stinson *et al.* (1982), Stinson (1990), and Voss and Allen (1994), the transformation of impedance to reflectance provides a measure of middle-ear response that does not depend on measurement location, assuming acoustic losses in the ear canal are negligible. Figure 8 (right) demonstrates that the reflectance magnitude, measured at any location within the ear canal, is sensitive to variations in the impedance of the middle-ear air space. Thus, as ear-canal middle-ear diagnostic tests are developed and evaluated, intersubject variations in middle-ear air space anatomy should be recognized as a source of variability in some ear-canal based measurements.

V. SUMMARY

Measurements of the impedance of the middle-ear air space from three cadaver ears with intact mastoid air spaces show a compliance-dominated impedance for frequencies lower than about 500 Hz and magnitudes with multiple extrema at higher frequencies. These measurements differ from previous measurements made on cadaver ears with altered mastoid spaces; ears with intact mastoid spaces have impedance magnitudes with multiple extrema, while ears with an enlarged antrum but no mastoid air-cell networks have impedances with fewer and sharper extrema. Previous models of the impedance of the middle-ear air space are consistent with the measurements on ears with no mastoid air-cell networks; the models represent the antrum and mastoid air cell system as a single volume of air. These models are able to capture the gross features of the impedance measurements presented here (e.g., the first magnitude miminum), but they fail to represent the multiple extrema in magnitude and corresponding transitions in angle. An alternative topology for a circuit model of the middle-ear air space is suggested as a guide for describing the acoustics of the middle-ear air space. However, the model's complexity and the substantial interear variability in the anatomy of the middle-ear air space make a specific model for the middle-ear air space impractical. In general, the previous models (Zwislocki, 1962; Kringlebotn, 1988; Voss *et al.*, 2000b) lose some of the fine structure in the impedance of the middle-ear air space but they provide a simple and reasonable approximation of this impedance.

Analysis of the measurements shows that variations in middle-ear air space impedance do affect the impedance at the tympanic membrane for frequencies above 1000 Hz. It is suggested that intersubject variability in ear-canal based measurements may result partially from variability in middle-ear air space anatomy.

ACKNOWLEDGMENTS

We gratefully thank Diane Jones of the Otopathology Laboratory of the Massachusetts Eye and Ear Infirmary for her assistance with preparing the temporal bones for measurements, John Kosakowski of the Smith College Machine Shop for his help in the design and building of the acoustic

cavities used to calibrate our system, and Rindy Northrop of The Temporal Bone Foundation, Inc. for sharing and viewing with us her sections prepared for microscopic observation of a human temporal bone that included the mastoid. We also thank John J. Rosowski, William T. Peake, and Christopher A. Shera for helpful discussions and comments on the manuscript. An anonymous reviewer also provided helpful comments on the manuscript. This work was the undergraduate Honor's Thesis of C.E.S. under the direction of Susan E. Voss. The research was supported by Smith College and a grant from the Ford Motor Company.

APPENDIX: CALCULATION OF MODEL ELEMENTS FOR THE FOUR-ELEMENT MODEL

We outline the process for determining the values for the four circuit elements (C_t, M_{ad}, R_{ad}, and C_a) of the model described in Fig. 1 (right). As presented by Voss *et al.* (2000b), we assume that at low frequencies, the cavity impedance Z_{CAV} can be approximated as a pure compliance C_{cav} which can be calculated from our measurements and used to constrain the compliances C_t and C_a such that

$$C_{cav} = C_t + C_a. \tag{A1}$$

We solve for C_{cav} from our measurements of Z_{CAV} at 244 Hz,

$$C_{cav}(f = 244\ \text{Hz}) = \left| \frac{1}{2\pi f Z_{CAV}} \right|. \tag{A2}$$

The parallel resonance between the mass M_{ad} and the compliances C_t and C_a leads to a maximum in $|Z_{CAV}|$ at the frequency f_{max} where[10]

$$f_{max} = \frac{1}{2\pi} \sqrt{\frac{C_t + C_a}{M_{ad} C_t C_a}}. \tag{A3}$$

The series resonance between M_{ad} and C_a leads to a minimum in $|Z_{CAV}|$ at the frequency f_{min} where

$$f_{min} = \frac{1}{2\pi} \sqrt{\frac{1}{M_{ad} C_a}}. \tag{A4}$$

Division of Eq. (A3) by Eq. (A4) gives

$$\frac{f_{max}}{f_{min}} = \sqrt{1 + (C_a/C_t)}. \tag{A5}$$

We can then compute values for C_a and C_t from Eqs. (A1) and (A5), with C_{CAV}, f_{max}, and f_{min} determined from the experimental data. With values for C_a and C_t, we use the frequency of the minimum in $|Z_{CAV}|$ and Eq. (A4) to solve for M_{ad}. Finally, we use a frequency-dependent resistance (Beranek 1986, pp. 137–138) that results in the magnitude of the measured $|Z_{CAV}|$ and the model $|Z_{CAV}|$ matching at the magnitude minimum, i.e., the resonant frequency between the mass M_{ad} and the compliances C_t and C_a.

[1]The measurements of middle-ear volume by Molvaer *et al.* (1978) include the tympanic cavity and the mastoid air cell system. We approximate the measurements of the mastoid air cell system to be approximately one cm^3 smaller than the reported measured volume of the entire space.

[2]The description provided by Onchi (1961) of the cadaver ear reads: "Pure tones were conducted by a metal tube into the external auditory canal of the temporal bones removed from fresh cadavers." Figure 3 of Onchi (1961) includes a schematic drawing of the antrum and mastoid-cell network which leads us to assume that the mastoid air cells were part of the ear on which Onchi (1961) measured Z_{CAV}.

[3]The measurements are noisy above 4000 Hz because the source used to measure the impedance did not generate sound pressure levels that were high enough to be sensed adequately by the microphone (Voss *et al.*, 2000b).

[4]The Zwislocki (1962) middle-ear air space model includes an additional resistor in parallel with the capacitor that represents the tympanic cavity within Fig. 1 (right). The additional resistor has been ignored for the discussion here, as it controls the sharpness of the resonances and does not add additional ones. This resistor is further discussed by Voss *et al.* (2000b).

[5]The two resonances are not obvious in the Kringlebotn (1988) model results (Fig. 2) because the model inductor value appears to be artificially low (Voss *et al.*, 2000b).

[6]We note that the two ears from the same cadaver resulted in the mastoid volumes of 5.9 cm^3 (ear 2) and 1.5 cm^3 (ear 3). A possible explanation for such asymmetry could be the observation that ears affected by secretory otitis media for substantial periods during the first years of life are smaller in volume than ventilated ears (Robinson *et al.*, 1993); perhaps the left ear of our cadaver donor was afflicted by otitis media during its developmental years.

[7]The impedance measurement made by Onchi (1961) on a single cadaver middle-ear air space was reproduced here as a magnitude and angle (Fig. 2) from the author's representation with a real and imaginary part. The original plot (Onchi, 1961, Fig. 10) suggests a noncausal response: Near 3000 Hz the real part of the impedance appears to be forced to maintain a positive value while there is no corresponding abrupt transition in the derivative of the imaginary part of the impedance at this frequency.

[8]We are unaware of systematic anatomical examinations to determine if connections between the tympanic cavity and the mastoid air-cell system in addition to the aditus ad antrum exist. However, in one set of serial temporal bone sections that we viewed, there appears to be a connection between the superior-anterior portion of the tympanic cavity and several air cells.

[9]Volume V is related to compliance C via the equation $V = \rho c^2 C$ where ρ is the density of air and c is the speed of sound in air.

[10]To simplify our expressions here, we initially ignore the effect of R_{ad}, which is small as shown by the sharp resonances in the measurements of Z_{CAV}.

Allen, J. B. (**1986**). "Measurement of eardrum acoustic impedance," in *Peripheral Auditory Mechanisms*, edited by J. B. Allen, J. L. Hall, A. Hubbard, S. T. Neely, and A. Tubis (Springer, Berlin), pp. 44–51.

Beranek, L. L. (**1986**). *Acoustics* (American Institute of Physics, New York).

Donaldson, J. A., Duckert, L. G., Lambert, P. M., and Rube, E. W. (**1992**). *Anson Donaldson Surgical Anatomy of the Temporal Bone*, 4th ed. (Raven, New York).

Farmer-Fedor, B. L. and Rabbitt, R. D. (**2002**). "Acoustic intensity, impedance and reflection coefficient in the human ear canal," J. Acoust. Soc. Am. **112**, 600–620.

Feeney, M. P., Grant, I. L., and Marryott, L. P. (**2003**). "Wideband energy reflectance measurements in adults with middle-ear disorders," J. Speech Lang. Hear. Res. **46**, 901–911.

Feeney, M. P. and Keefe, D. H. (**1999**). "Acoustic reflex detection using wideband acoustic reflectance, admittance, and power measurements," J. Speech Lang. Hear. Res. **42**, 1029–1041.

Feeney, M. P. and Keefe, D. H. (**2001**). "Estimating the acoustic reflex threshold from wideband measures of reflectance, admittance, and power," Ear Hear.. **22**, 316–332.

Goode, R. L., Ball, G., and Nishihara, S. (**1993**). "Measurement of umbo vibration in human subjects—method and possible clinical applications," Am. J. Otol. **14**, 247–251.

Gyo, K., Goode, R. L., and Miller, C. (**1986**). "Effect of middle-ear modification on umbo vibration—human temporal bone experiments with a new vibration measuring system," Arch. Otolaryngol. Head Neck Surg. **112**, 1262–1268.

Huang, G. T., Rosowski, J. J., Flandermeyer, D. T., Lynch, T. J., and Peake, W. T. (**1997**). "The middle ear of a lion: Comparison of structure and function to domestic cat," J. Acoust. Soc. Am. **101**, 1532–1549.

Huang, G. T., Rosowski, J. J., Puria, S., and Peake, W. T. (**2000**). "A non-

invasive method for estimating acoustic admittance at the tympanic membrane," J. Acoust. Soc. Am. **108**, 1128–1146.
Hunter, L. L. and Margolis, R. H. (**1997**). "Effects of tympanic membrane abnormalities on auditory function," J. Am. Acad. Audiol **8**, 431–446.
Keefe, D. H. (**1984**). "Acoustical wave propagation in cylindrical ducts: Transmission line parameter approximations for isothermal and nonisothermal boundary conditions," J. Acoust. Soc. Am. **75**, 58–62.
Keefe, D. H., Bulen, J. C., Arehart, K. H., and Burns, E. M. (**1993**). "Ear-canal impedance and reflection coefficient in human infants and adults," J. Acoust. Soc. Am. **94**, 2617–2638.
Keefe, D. H. and Levi, E. C. (**1996**). "Maturation of the middle and external ears: Acoustic power-based responses and reflectance tympanometry," Ear Hear. **17**, 361–373.
Koç, A., Ekinci, G., Bilgili, A. M., Akpinar, I. N., Yakut, H., and Han, T. (**2003**). "Evaluation of the mastoid air cell system by high resolution computed tomography: Three-dimensional multiplanar volume rendering technique," J. Laryngol. Otol. **117**, 595–598.
Kringlebotn, M. (**1988**). "Network model for the human middle ear," Scand. Audiol. **17**, 75–85.
Magliulo, G., Cianfrone, G., Gagliardi, M., Cuiuli, G., and D'Amico, R. (**2004**). "Vestibular evoked myogenic potentials and distortion-product otoacoustic emissions combined with glycerol testing in endolymphatic hydrops: Their value in early diagnosis," Ann. Otol. Rhinol. Laryngol. **15**, 1000–1005.
Margolis, R. H., Saly, G. L., and Keefe, D. H. (**1999**). "Wideband reflectance tympanometry," J. Acoust. Soc. Am. **106**, 265–280.
Merchant, S. N., Ravicz, M. E., Puria, S., Voss, S. E., Whittemore, Jr., K. R., Peake, W. T., and Rosowski, J. J. (**1997**). "Analysis of middle-ear mechanics and application to diseased and reconstructed ears," Am. J. Otol. **18**, 139–154.
Merchant, S. N., Ravicz, M. E., Voss, S. E., , Peake, W. T., and Rosowski, J. J. (**1998**). "Middle ear mechanics in normal, diseased, and reconstructed ears," J. Laryngol. Otol. **112**, 715–731.
Merchant, S. N., Rosowski, J. J., and Ravicz, M. E. (**1995**). "Middle ear mechanics of type IV and type V tympanoplasty. II. Clinical analysis and surgical implications," Am. J. Otol. **16**, 565–575.
Møller, A. R. (**2000**). *Hearing: Its Physiology and Pathophysiology* (Academic, San Diego).
Molvaer, O., Vallersnes, F., and Kringlebotn, M. (**1978**). "The size of the middle ear and the mastoid air cell," Acta Oto-Laryngol. **85**, 24–32.
Neely, S. T. and Gorga, M. P. (**1998**). "Comparison between intensity and pressure as measures of sound level in the ear canal," J. Acoust. Soc. Am. **104**, 2925–2934.
Onchi, Y. (**1961**). "Mechanism of the middle ear," J. Acoust. Soc. Am. **33**, 794–805.
Piskorski, P., Keefe, D. H., Simmons, J. L., and Gorga, M. P. (**1999**). "Prediction of conductive hearing loss based on acoustic ear-canal response using a multivariate clinical decision theory," J. Acoust. Soc. Am. **105**, 1749–1764.
Robinson, P. J., Lodge, S., Goligher, J., Bowley, N., and Grant, H. R. (**1993**). "Secretory otitis media and mastoid air cell development," Int. J. Pediatr. Otorhinolaryngol. **25**, 13–18.
Rosowski, J. J., Davis, P. J., Merchant, S. N., Donahue, K. M., and Coltrera, M. D. (**1990**). "Cadaver middle ears as models for living ears: Comparisons of middle ear input impedance," Ann. Otol. Rhinol. Laryngol. **99**, 403–412.
Rosowski, J. J. and Merchant, S. N. (**1995**). "Mechanical and acoustic analysis of middle ear reconstruction," Am. J. Otol. **16**, 486–497.
Rosowski, J. J., Merchant, S. N., and Ravicz, M. E. (**1995**). "Middle ear mechanics of type IV and type V tympanoplasty. I. Model analysis and predictions," Am. J. Otol. **16**, 555–564.
Schuknecht, H. (**1968**). "Temporal bone removal at autopsy," Arch. Otolaryngol. **87**, 129–137.
Stepp, C. E. and Voss, S. E. (**2004**). "Acoustics of the middle-ear air space in human ears," Abstracts of the American Auditory Society Annual Meeting, Vol. **29**.
Stinson, M. R. (**1990**). "Revision of estimates of acoustic energy reflectance at the human eardrum," J. Acoust. Soc. Am. **88**, 1773–1778.
Stinson, M. R., Shaw, E., and Lawton, B. W. (**1982**). "Estimation of acoustical energy reflectance at the eardrum from measurements of pressure distribution in the human ear canal," J. Acoust. Soc. Am. **72**, 766–773.
Voss, S. E. (**1998**). "Effects of tympanic-membrane perforations on middle-ear sound transmission: Measurements, mechanisms, and models," Ph.D. thesis, Massachusetts Institute of Technology.
Voss, S. E. and Allen, J. B. (**1994**). "Measurement of acoustic impedance and reflectance in the human ear canal," J. Acoust. Soc. Am. **95**, 372–384.
Voss, S. E., Rosowski, J. J., Merchant, S. N., and Peake, W. T. (**2001a**). "How do tympanic-membrane perforations affect human middle-ear sound transmission?," Acta Oto-Laryngol. **121**, 169–173.
Voss, S. E., Rosowski, J. J., Merchant, S. N., and Peake, W. T. (**2001b**). "Middle-ear function with tympanic-membrane perforations. I. Measurements and mechanisms," J. Acoust. Soc. Am. **110**, 1432–1444.
Voss, S. E., Rosowski, J. J., Merchant, S. N., and Peake, W. T. (**2001c**). "Middle-ear function with tympanic-membrane perforations. II. A simple model," J. Acoust. Soc. Am. **110**, 1445–1452.
Voss, S. E., Rosowski, J. J., Merchant, S. N., and Peake, W. T. (**2000b**). "Acoustic responses of the human middle ear," Hear. Res. **150**, 43–69.
Voss, S. E., Rosowski, J. J., Merchant, S. N., Thornton, A. R., Shera, C. A., and Peake, W. T. (**2000c**). "Middle-ear pathology can affect the ear-canal sound pressure generated by audiologic earphones," Ear Hear. **21**, 265–274.
Voss, S. E., Rosowski, J. J., Shera, C. A., and Peake, W. T. (**2000a**). "Acoustic mechanisms that determine the ear-canal sound pressures generated by earphones," J. Acoust. Soc. Am. **107**, 1548–1565.
Voss, S. E. and Shera, C. A. (**2004**). "Simultaneous measurement of middle-ear input impedance and forward/reverse transmission in cat," J. Acoust. Soc. Am. **110**, 2187–2198.
Whittemore, K. R., Merchant, S. N., and Rosowski, J. J. (**1998**). "Acoustic mechanisms. Canal wall-up versus canal wall-down mastoidectomy," Otolaryngol.-Head Neck Surg. **118**, 751–761.
Zwislocki, J. (**1962**). "Analysis of the middle-ear function. 1. Input impedance," J. Acoust. Soc. Am. **34**, 1514–1523.
Zwislocki, J. and Feldman, A. (**1970**). "Acoustic impedance in normal and pathological ears," Am. Speech Hear. Assoc. Monograph **15**, 1–42.